



Dendritic Synchrony and Transient Dynamics in a Coupled Oscillator Model of the Dopaminergic Neuron

G.S. MEDVEDEV*

Program in Applied and Computational Mathematics, Princeton University, Princeton, NJ 08544-1000, USA; School of Mathematics, Institute for Advanced Study, Einstein Drive, Princeton, NJ 08540, USA

medvedev@mcs.drexel.edu

C.J. WILSON

Cajal Neuroscience Center, Division of Life Sciences, University of Texas at San Antonio, San Antonio, TX 78249, USA

CJWILSON@utsa.edu

J.C. CALLAWAY

Department of Anatomy and Neurobiology, University of Tennessee Health Science Center, Memphis, TN 38163, USA

jcallaway@utmem.edu

N. KOPELL

Department of Mathematics and Center for BioDynamics, Boston University, 111 Cummington Street, Boston, MA 02215, USA

nk@math.bu.edu

Received August 13, 2002; Revised December 31, 2002; Accepted February 11, 2003

Action Editor: John R. Huguenard

Abstract. Transient increases in spontaneous firing rate of mesencephalic dopaminergic neurons have been suggested to act as a reward prediction error signal. A mechanism previously proposed involves subthreshold calcium-dependent oscillations in all parts of the neuron. In that mechanism, the natural frequency of oscillation varies with diameter of cell processes, so there is a wide variation of natural frequencies on the cell, but strong voltage coupling enforces a single frequency of oscillation under resting conditions. In previous work, mathematical analysis of a simpler system of oscillators showed that the chain of oscillators could produce transient dynamics in which the frequency of the coupled system increased temporarily, as seen in a biophysical model of the dopaminergic neuron. The transient dynamics was shown to be consequence of a slow drift along an invariant subset of phase space, with rate of drift given by a Lyapunov function. In this paper, we show that the same mathematical structure exists for the full biophysical model, giving physiological meaning to the slow drift and the Lyapunov function, which is shown to describe differences in intracellular calcium concentration in different parts of the cell. The duration of transients

*Present address: Department of Mathematics and Computer Science, 206 Korman Center, Drexel University, Philadelphia, PA 19104, USA.

was long, being comparable to the time constant of calcium disposition. These results indicate that brief changes in input to the dopaminergic neuron can produce long lasting firing rate transients whose form is determined by intrinsic cell properties.

Keywords: dopaminergic neuron, basal ganglia, coupled oscillator model, transient dynamics, synchronization

1. Introduction

Wilson and Callaway suggested a new approach to generating firing patterns of dopaminergic neurons in the mammalian brain stem (Wilson and Callaway, 2000). The spontaneous firing patterns of these neurons are important in maintaining physiological levels of dopamine release in the mammalian striatum, which is essential for the generation of voluntary movements. Perturbations in the spontaneous firing of the neurons have been proposed to act as a reward prediction error signal, with transient increases signaling unpredicted rewards and transient decreases in firing signaling the absence of a predicted reward (Waelti et al., 2001). These transient changes in firing are expected to result from changes in synaptic input, but the mechanisms determining their time course are not known. Using a biophysically based compartmental model of the dopaminergic neuron, Wilson and Callaway showed that experimentally verified differences in the dynamics of calcium disposition imply variation in natural frequency of the oscillator mechanism along the dendrites of the cell. In computer simulations, interactions among dendritic regions with different natural frequencies strongly influenced the firing rate transient to a step change in input current. It was suggested that this mechanism may help to shape the natural response transients in dopaminergic neurons.

Inspired by that paper, Medvedev and Kopell undertook a mathematical investigation of a more abstract model of the cell, also described as a chain of oscillators (Medvedev and Kopell, 2001). In that work, each oscillator had a geometry that was roughly the same as that of a model compartment in the work of Wilson and Callaway. The oscillators studied by Medvedev and Kopell were FitzHugh-Nagumo equations, in the relaxation regime. Medvedev and Kopell showed that a chain of these oscillators produce very similar transient increases in frequency when the system is started with the fast variable (voltage in the biophysical model) initially set to a low and uniform value. Furthermore, the model was amenable to understanding the mechanistic origins of the transient behavior: the analysis revealed that, in the limit of strong coupling (the relevant regime

for the biophysical model), the system has a memory for initial conditions (Medvedev and Kopell, 2001). If the coupling is large but not infinite, the system drifts slowly (the transient behavior) toward a steady state oscillation at a lower frequency. The work had the anti-intuitive result that stronger coupling could produce longer transients.

The results of Medvedev and Kopell (2001) could not be applied directly to the model of Wilson and Callaway (2000) because it apparently made use of specific features of the FitzHugh-Nagumo model. The purpose of this paper is to show that similar techniques to those of Medvedev and Kopell (2001) do indeed apply to a large class of equations including those of Wilson and Callaway (2000), enabling one to understand the origin of the transient dynamics in the biophysical case. In the process, one gets a much clearer view of which parameters of the biophysical system govern the time scale of the transient response. The analysis also accounts for details of the dynamics, as stated in the next section. In particular, it yields the forms and the common frequency of Ca-oscillations along the dendrite, and explains the variation in the amplitudes of Ca-oscillations.

In Section 2 we give the biophysical model of Wilson and Callaway (2000) to be analyzed here. Sections 3 and 4 contain the main analysis, especially for large values of electrical coupling between the compartments. The analysis is done for two compartments. As shown by Medvedev and Kopell (2001), this can be extended to an arbitrary number of compartments; however, the extension is technical, and we restrict the exposition of the analysis to two compartments to put the focus on the new effects introduced by working with a physiological model instead of an abstract model. To emphasize that the dynamics under investigation as well as our working assumptions hold for multi-compartment models, simulations are presented for a model with five compartments.

Section 3 shows that the four-dimensional phase space of the two-compartment model contains, in the limit of large coupling strength g , an attracting two-dimensional cylinder parameterized by slow variables u_1 and u_2 . This cylinder is foliated into a one-parameter

family of limit cycles. In Section 4, we analyze the case of large, but not infinite, coupling strength, and show that there is a drift along the cylinder. The rate of drift, which gives the time scale of the transient response, is calculated. From the calculation, we see that there are parameter regimes, as in Medvedev and Kopell (2001), for which the time of the transient is proportional to the coupling strength. However, we also see that other features of the physiology can dominate in some regimes, and we interpret the calculations to see which ones.

2. Biophysical Model of the Dopaminergic Neuron

The model introduced by Wilson and Callaway (2000) describes the interaction of voltage and calcium concentration in a multi-compartment model of the dendrite. The variables for each compartment are $v_i(t)$, the voltage, and $u_i(t)$, the calcium concentration, taken to be uniform throughout the compartment. (For elaborations on this model, we refer the reader to the paper of Wilson and Callaway, 2000.) The dynamics of the voltage variables are determined by the current balance equations in individual compartments:

$$\frac{dv_i}{dt} = \frac{1}{C} (g_{Ca}(v_i)(E_{Ca} - v_i) + g_{KCa}(u_i)(E_K - v_i) + g_l(E_l - v_i) + G_i(v_{i+1} - 2v_i + v_{i-1})),$$

$$i = 1, 2, \dots, N, \quad (2.1)$$

and no-flux boundary conditions: $v_0 = v_1$, $v_N = v_{N+1}$. The first three terms in (2.1) represent intrinsic currents of the compartment: a voltage-gated calcium current, a calcium-gated potassium current, and a leak current. C is the capacitance. The last term models the electrical coupling between neighboring compartments. The conductivity G_i between two adjacent compartments is calculated by

$$G_i = \frac{\pi d_i^2}{Rh},$$

where d_i is the diameter of the cross section of a cylindrical compartment, R is the longitudinal resistivity of the cytoplasm, and h is the compartment length. The strength of the coupling depends on the diameter of the compartment and varies along the chain. For analytical convenience we factor G_i into a product of two terms $g\rho_i^2$, where $g = \frac{\pi d_{\text{soma}}^2}{Rh}$ and $\rho_i = \frac{d_i}{d_{\text{soma}}}$. The first term represents the conductivity (the strength of coupling) between the somatic compartment and the next one, the weights ρ_i rect the variation of the strength of coupling along the dendrite.

The conductances $g_{Ca}(v)$ and $g_{KCa}(u)$ are given by the formulas

$$g_{Ca}(v) = \frac{\overline{g_{Ca}}}{1 + e^{\frac{-(v+35)}{7}}}, \quad (2.2)$$

$$g_{KCa}(u) = \frac{\overline{g_{KCa}}u^4}{u^4 + k^4}. \quad (2.3)$$

Here, constants 35 and 7 (both in mV) are the half-activation voltage and the slope factor, respectively. Constant k in Eq. (2.3) is the half activation concentration for the calcium-dependent conductance. Figure 1 shows the functional forms of $g_{Ca}(v)$ and $g_{KCa}(u)$. We will also need to refer to the voltage equation in an individual (uncoupled) compartment, i.e. to Eq. (2.1) with $G_i = 0$. For this equation, we reserve a label (2.1)₀.

The equation for the calcium concentration in the i th compartment is

$$\frac{du_i}{dt} = \frac{g_{Ca}(v_i)(E_{Ca} - v_i)4\beta}{zFd_i} - \frac{P_{\max}4\beta u_i}{d_i}. \quad (2.4)$$

Here, z is the valence of calcium, F is Faraday's constant, β is the ratio of free to buffered calcium, P_{\max} is the maximum pump rate surface density. d_i denotes the diameter of compartment i .

The parameters are given in Table 1.

In addition, for our numerical simulations we have chosen a five-compartment model ($N = 5$) with $d_{\text{soma}} = 16 \mu\text{m}$ and exponential tapering of the dendritic compartments: $\rho_i = 2^{-i+1}$, $i = 1, 2, \dots, 5$.

A phase plane analysis for a single uncoupled oscillator (2.1)₀, (2.4) shows that it has an attracting limit

Table 1. Model parameters.

E_{Ca}	100	mV	E_K	-90	mV	E_l	-50	mV	P_{\max}	2000	$\frac{\mu\text{m}}{\text{s}}$
g_l	0.1	$\frac{\text{mS}}{\text{cm}^2}$	$\overline{g_{Ca}}$	0.08	$\frac{\text{mS}}{\text{cm}^2}$	g_{KCa}	0.2	$\frac{\text{mS}}{\text{cm}^2}$	k	180	nM
C	1	$\frac{\mu\text{F}}{\text{cm}^2}$	β	0.001		h	30	μm	R	100	ohm-cm

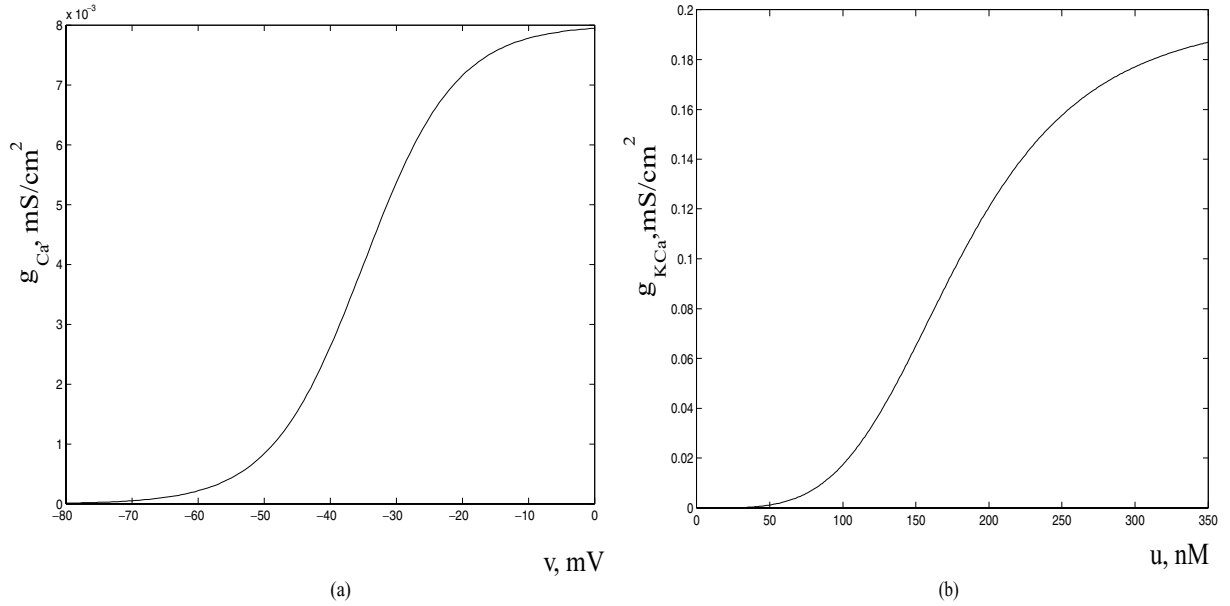


Figure 1. The nonlinear conductances used in Eq. (2.1): (a) the voltage-dependent calcium conductance $g_{Ca}(v)$, ($\frac{\text{mS}}{\text{cm}^2}$) and (b) the calcium-dependent potassium conductance $g_{KCa}(u)$, ($\frac{\text{mS}}{\text{cm}^2}$).

cycle (Fig. 2a). Consequently, after an initial period of time, solutions of (2.1)₀, (2.4) undergo oscillations as shown in Figs. 2b and c. The segments of rapid changes of $v_i(t)$ and $u_i(t)$ reflect multiple time scales. In fact, an inspection of the parameters of the system reveals that the range of the values of the right hand side of the voltage equation is at least tenfold greater than those of the calcium equations. For this reason, the voltage equation is referred to as a fast equation, and the oscillator (2.1)₀, (2.4) is a relaxation oscillator. Normally, a system in relaxation regime can be recognized by the presence of a small parameter. Such parameter can be derived in our case too if we non-dimensionalize our equations. However, we prefer to work with original equations in order to be able to keep track of the physiological meaning of various parameters.

Thus, each compartment of our model represents a relaxation oscillator with phase plane as shown on Fig. 2a. The right hand sides of (2.4) are proportional to d_i^{-1} . The latter varies along the chain of compartments. As a result, the natural frequencies of oscillations in different compartments are different. Nonetheless, the solutions of the coupled system ($G_i > 0$) exhibit oscillations at a common frequency. In particular, in our numerical example the voltage variables in all five compartments oscillate synchronously and are almost identical (Fig. 3a). Calcium concentration vari-

ables oscillate in phase with voltages, but the amplitudes of calcium oscillations in different compartments are drastically different with the largest amplitudes in the distal dendritic compartment. In addition the time series plots of calcium variables (Fig. 3b) show pronounced transient dynamics, during which the average calcium concentrations over one cycle of oscillations in all compartments slowly evolve towards a common value. Similar transient behavior can be clearly seen in the experimental data (Wilson and Callaway, 2000). It is useful to consider the projections of the trajectory onto the phase planes of individual compartments ($v_i - u_i$). Such plots for the first (somatic) and the last (distal dendritic) compartments are given in Figs. 3c and d. If we ignore the self-intersections of the trajectory projections, these phase planes are very similar to that of a single relaxation oscillator. The analogy of the dynamics of the coupled system to that of a single oscillator is very fruitful for understanding the system's behavior. The analysis of the following section is built on this analogy.

Heuristically, the synchronous behavior of solutions of (2.1) and (2.4) can be explained by strong electrical coupling in (2.1). However, the precise mechanism of synchronization is far from obvious and its understanding requires mathematical analysis. The basic questions about the solutions of (2.1) and (2.4),

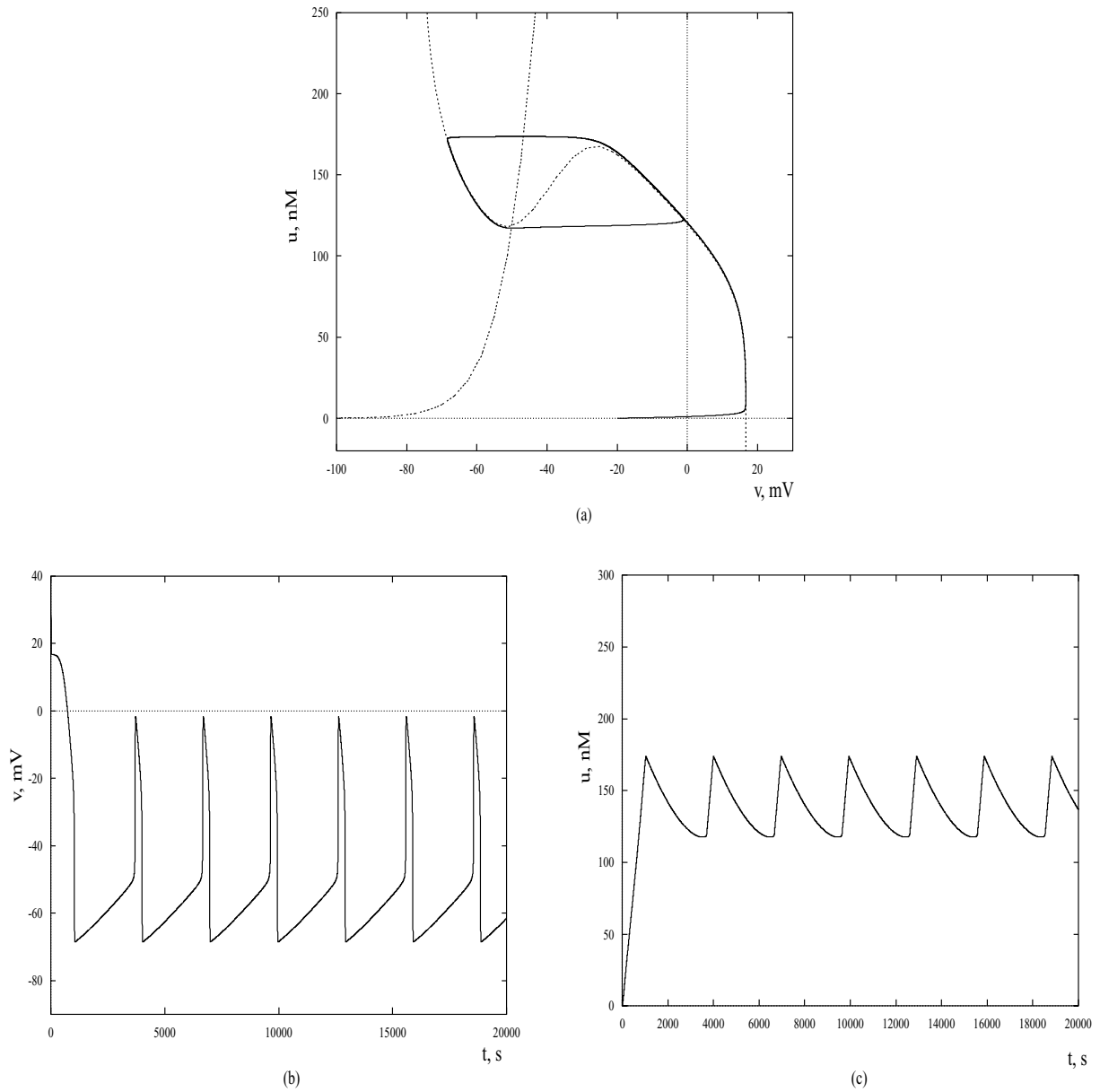


Figure 2. (a) Phase plane of the relaxation oscillator (2.1)₀, (2.4): two dashed curves represent nullclines for the voltage and calcium equations, i.e. the sets of points where $\frac{dv_i}{dt} = 0$ (S-shaped curve) and $\frac{du_i}{dt} = 0$ respectively. The bold line depicts a typical trajectory. The closed part of trajectory encircles a limit cycle. After initial period of time, a phase point is going around the limit cycle. Consequently, the time series plots of the voltage variable (b) and the calcium concentration variable (c) exhibit periodic oscillations.

which we would like to answer are: how is the common frequency of coupled oscillations formed, what determines the variation of amplitudes of calcium oscillations, and what is the origin and duration of transients. We answer these questions by extending the analysis for chains of coupled FitzHugh-Nagumo os-

illators (Medvedev and Kopell, 2001). The results of Medvedev and Kopell (2001), though relevant, do not apply directly to Eqs. (2.1) and (2.4). Besides the problems connected with this extension, the main concern of this paper is physiological interpretation of the analytical results.

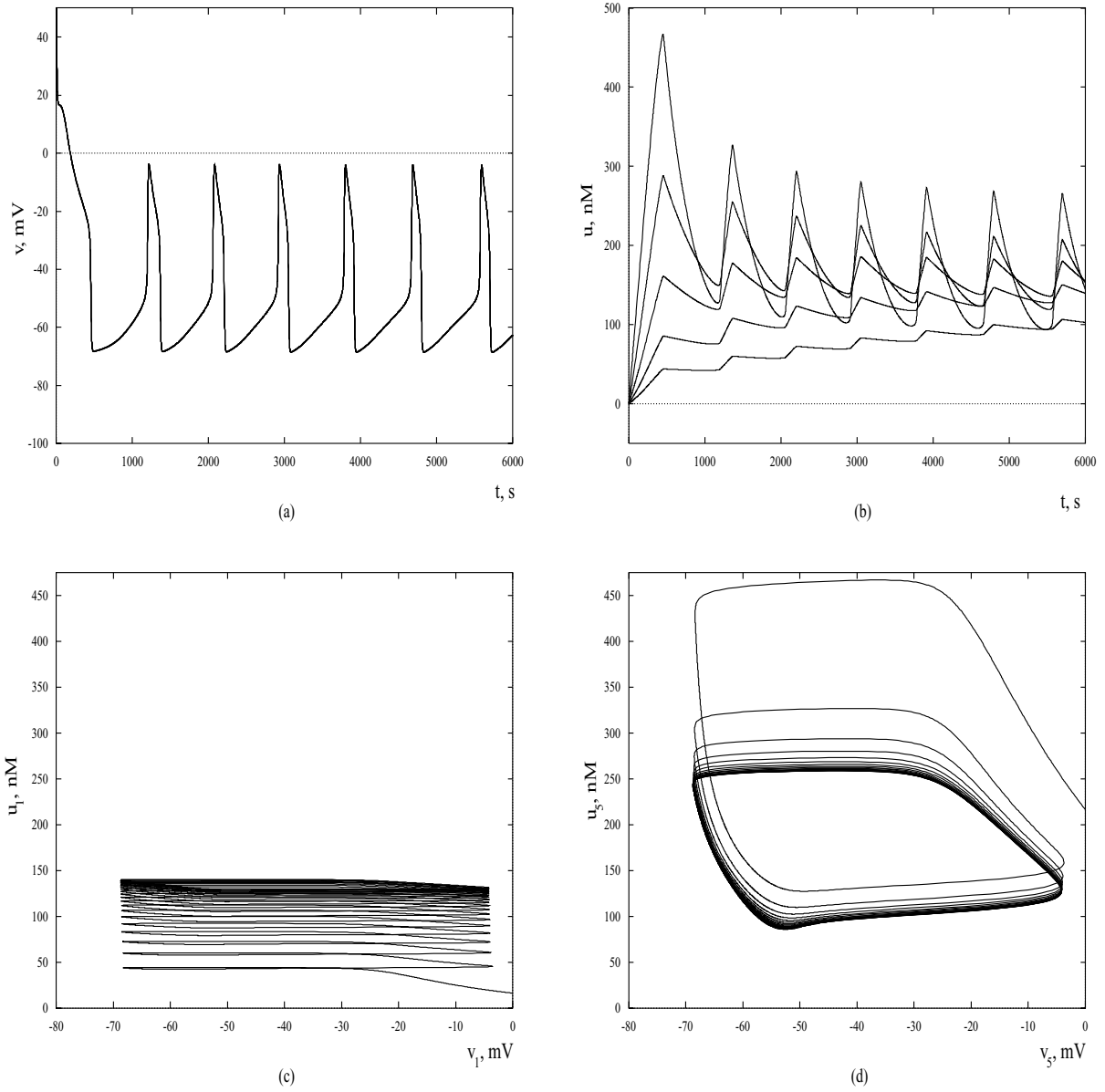


Figure 3. (a) The time series plots of v_i 's ($i = 1, 2, \dots, 5$) in a five-compartment model. The voltages in different compartments are almost identical. (b) The time series plots of the calcium concentration variables: the calcium oscillations are in phase with voltages, but they have different amplitudes in different compartments. The mean values of the calcium concentrations slowly converge to a common value for all compartments. (c, d) Projections of the phase trajectory onto the phase planes of the first (c) and the 5th (d) oscillators.

3. Model Behavior in the Limit of Strong Coupling

In this and the next sections we analyze the system of Eqs. (2.1) and (2.4). In general, solving a system of $2N$ nonlinear ordinary differential equations such as the system at hand is a highly nontrivial task. Fortu-

nately, the problem can be considerably simplified if the coupling is strong ($g \gg 1$). The parameter values (Table 1) suggest that this is the relevant regime in our case. This can also be verified numerically: increasing g does not lead to any noticeable change in the system's dynamics. In this section, we derive approximate simplified equations for the dynamics when $g \gg 1$. For

the sake of simplicity of presentation, we consider only two coupled compartments: somatic and dendritic. A general N -compartment model can be dealt with in a similar manner.

We rewrite Eqs. (2.1) and (2.4) for two compartments, and make an approximation based on Fig. 1 and numerics. The approximation uses the fact that the calcium concentration range of the oscillations is between 50 and 300 nM. From Fig. 1, we see that in this range the function $g_{\text{KCa}}(u)$ is almost linear. Thus, we write

$$\frac{g_{\text{KCa}}(u)}{C} = -\alpha u + \sigma, \quad (3.1)$$

where $\alpha = -10^{-3} \frac{\text{mS}}{\text{cm}^2 \text{nM}}$ and $\sigma = 0.08 \frac{\text{mS}}{\text{cm}^2}$.

We use this to write the current balance equations for the two compartments as

$$\frac{dv_1}{dt} = \tilde{F}(v_1) - \alpha u_1(E_K - v_1) + rg(v_2 - v_1), \quad (3.2)$$

$$\frac{dv_2}{dt} = \tilde{F}(v_2) - \alpha u_2(E_K - v_2) - lg(v_2 - v_1), \quad (3.3)$$

where $r, l = \frac{\pi d_{1,2}^2}{Rh}$ and

$$\tilde{F}(v) = \frac{1}{C}(g_{\text{Ca}}(v)(E_{\text{Ca}} - v) + g_l(E_l - v) + \sigma(E_K - v)) \quad (3.4)$$

is the calcium independent component of membrane current density due to ion channels in the compartment (not including coupling currents). The last terms on the right hand sides of Eqs. (3.2) and (3.3) account for the transmembrane current density due to coupling current.

The equation for $\frac{du}{dt}$ can be written as

$$\frac{du_i}{dt} = \omega_i(G(v_i) - \gamma u_i), \quad i = 1, 2. \quad (3.5)$$

$\omega_i = \frac{4\beta}{d_i}$ is a filling rate. It is the rate at which calcium flux will change the intracellular concentration of calcium. $G(v) = \frac{g_{\text{Ca}}(v)(E_{\text{Ca}} - v)}{zF}$ is calcium flux per unit surface area due to the calcium channel. It is the counterpart of $\gamma u = P_{\text{max}}u$, which is calcium flux per unit surface area due to the pump.

As we have already mentioned in the previous section, with parameter values in Table 1 Eqs. (2.1) and (2.4) are in the relaxation regime. This means that the dynamics of (2.1) and (2.4) can be split into two alternating modes: slow motions and fast jumps. Standard

results from the theory for singularly perturbed differential equations (Mishchenko et al., 1994) imply that the slow motion is taking place on the stable portions of the slow manifolds, that, with good accuracy, can be approximated by the following equations

$$u_1 = \frac{\tilde{F}(v_1)}{\alpha(E_K - v_1)} + \frac{rg(v_2 - v_1)}{\alpha(E_K - v_1)}, \quad (3.6)$$

$$u_2 = \frac{\tilde{F}(v_2)}{\alpha(E_K - v_2)} + \frac{lg(v_1 - v_2)}{\alpha(E_K - v_2)}. \quad (3.7)$$

These equations were formally obtained by setting to zero $\frac{dv_i}{dt}$, $i = 1, 2$ in (3.2) and (3.3). Equation (3.5) define the law of motion on the stable portions of the slow manifold. Equations (3.5)–(3.7) fully characterize the slow dynamics of solutions of (3.2)–(3.5). They are known as the “singular” slow equations: they are increasingly accurate the more the voltage equations have terms much larger than those of the calcium equation.

Equations (3.6) and (3.7) describe a two-dimensional surface in a four-dimensional space. It is hard to understand the geometry of the slow manifolds, because of the high dimensionality of the phase space. The situation becomes even more complex when the number of oscillators is greater than two. To overcome this difficulty, we simplify the equations for the slow manifolds. This simplification is possible in the regime when the coupling is strong ($g \gg 1$). It is accomplished via the asymptotic analysis as $\delta = \frac{1}{g} \rightarrow 0$. This procedure was developed and rigorously justified for chains of FitzHugh-Nagumo oscillators in Medvedev and Kopell (2001). Here we describe the main steps of this asymptotic analysis applied to the biophysical model (3.2)–(3.5). For more technical details, an interested reader should see the appendix to this paper.

The asymptotic analysis that follows relies on the following ansatz:

$$v_2 - v_1 = O(\delta), \quad \delta = \frac{1}{g}. \quad (3.8)$$

Equation (3.8) says that the strong electrical coupling in (3.2)–(3.5) pulls two voltage variables together in such a way that the coupling terms $rg(v_2 - v_1)$ and $lg(v_1 - v_2)$ are both $O(1)$ as g increases without bound:

$$\frac{g(v_2 - v_1)}{\alpha(E_K - v_1)} \approx \frac{g(v_2 - v_1)}{\alpha(E_K - v_2)} = O(1).$$

For each time interval that the phase point (v_1, u_1, v_2, u_2) spends on the slow manifold we define a function

$c(v_1)$ along the phase trajectory $(v_1(t), u_1(t), v_2(t), u_2(t))$, $t \in \mathbb{R}^+$:

$$c(v_1) \equiv \frac{g(v_2 - v_1)}{\alpha(E_K - v_1)}, \quad (3.9)$$

where $c(v_1)$ is $O(1)$ as $g \rightarrow \infty$. Function $c(v_1)$ determines the coupling current in the first compartment. In view of (3.8), it also approximates (up to a factor of l) the coupling current in the second compartment:

$$\frac{g(v_2 - v_1)}{\alpha(E_K - v_2)} \approx c(v_1), \quad (3.10)$$

when g is sufficiently large. Using (3.9) and (3.10) we can rewrite (3.6) and (3.7) as

$$u_1 = f(v_1) + rc(v_1), \quad (3.11)$$

$$u_2 = f(v_1) - lc(v_1), \quad (3.12)$$

where

$$f(v) = \frac{\tilde{F}(v)}{\alpha(E_K - v)}. \quad (3.13)$$

The last terms on the right hand sides of Eqs. (3.11) and (3.12), which involve $c(v_1)$, can be interpreted as changes to the voltage-dependent equilibrium values of calcium due to the coupling current. Equations (3.11)–(3.13) approximate the slow manifolds for (3.2)–(3.5), provided the function $c(v_1)$ is known. Equations (3.11) and (3.12) are uncoupled. Therefore, combined with (3.5) they can be considered as a pair of uncoupled relaxation oscillators. The latter are easy to analyze. Thus, our next task is to find $c(v_1)$.

The function $c(v_1)$ in (3.7) can be made explicit by using Eqs. (3.5), (3.11), and (3.12). By differentiating both sides of (3.11) and (3.12) with respect to v_1 , we obtain

$$\frac{du_1}{dv_1} = f'(v_1) + rc'(v_1), \quad (3.14)$$

$$\frac{du_2}{dv_1} = f'(v_1) - lc'(v_1). \quad (3.15)$$

From the other constraint, Eq. (3.5), we obtain

$$\frac{du_i}{dv_1} = \omega_i(G(v_1) - \gamma u_i) \left(\frac{dv_1}{dt} \right)^{-1}, \quad i = 1, 2. \quad (3.16)$$

We divide Eq. (3.14) by (3.15) and take a similar ratio for $i = 1, 2$ of (3.16). By setting these two ratios equal,

we obtain

$$\frac{f'(v_1) + rc'(v_1)}{f'(v_1) - lc'(v_1)} = \frac{\omega_1(G(v_1) - \gamma u_1)}{\omega_2(G(v_1) - \gamma u_2)}. \quad (3.17)$$

We wish to solve (3.17) for $c(v_1)$. Note that the explicit dependence of (3.17) on the u_i can be removed by using (3.11) and (3.12). Simple algebra then yields a complicated ordinary differential equation for $c(v_1)$, which we do not give. Instead, we use the following approximation. Simulations show that, for the parameters of our system, the right hand side of (3.17) is approximately independent of the u_i on the slow portions of the trajectory; i.e., the right hand side is approximately $\frac{\omega_1}{\omega_2}$. In Fig. 4, we plot the numerical values of the ratios $\chi_i = \frac{G(v_i) - \gamma u_i}{G(v_{i+1}) - \gamma u_{i+1}}$, $i = 1, 2$ for the five-compartment model. One can see that, away from the moments of time when the denominators $G(v_i) - \gamma u_i$ are singular, these ratios are almost constant and close to 1. The ratios for the last two compartments are not as close to 1 as those shown in the Fig. 4, but they are still in the range of 0.75–1.25 for the most part of the slow motion. In our analysis, we will assume

$$\frac{G(v_1) - \gamma u_1}{G(v_1) - \gamma u_2} \approx 1. \quad (3.18)$$

In Section 4, we will validate this assumption. Using simplifying assumption (3.18), we solve (3.17):

$$c'(v_1) = \xi f'(v_1), \quad \xi = \frac{\omega_1 - \omega_2}{l\omega_1 + r\omega_2}. \quad (3.19)$$

which implies that

$$c(v_1) = \xi f(v_1) + K. \quad (3.20)$$

Here K is an arbitrary constant of integration. Using (3.20), (3.11) and (3.12), we obtain

$$u_1 = (1 + r\xi)f(v_1) + rK, \quad (3.21)$$

$$u_2 = (1 - l\xi)f(v_1) - lK. \quad (3.22)$$

If K is fixed, Eqs. (3.21) and (3.22) allow us to describe the dynamics of the coupled system in terms of that of a single relaxation oscillator. As in a single oscillator case (see Fig. 2a), Eqs. (3.21) and (3.22) determine the generalized nullclines in the $v_1 - u_1$ and $v_1 - u_2$ phase planes respectively (Fig. 5). These nullclines, combined with the dynamical equations (3.5), describe the system's dynamics with good accuracy. In particular,

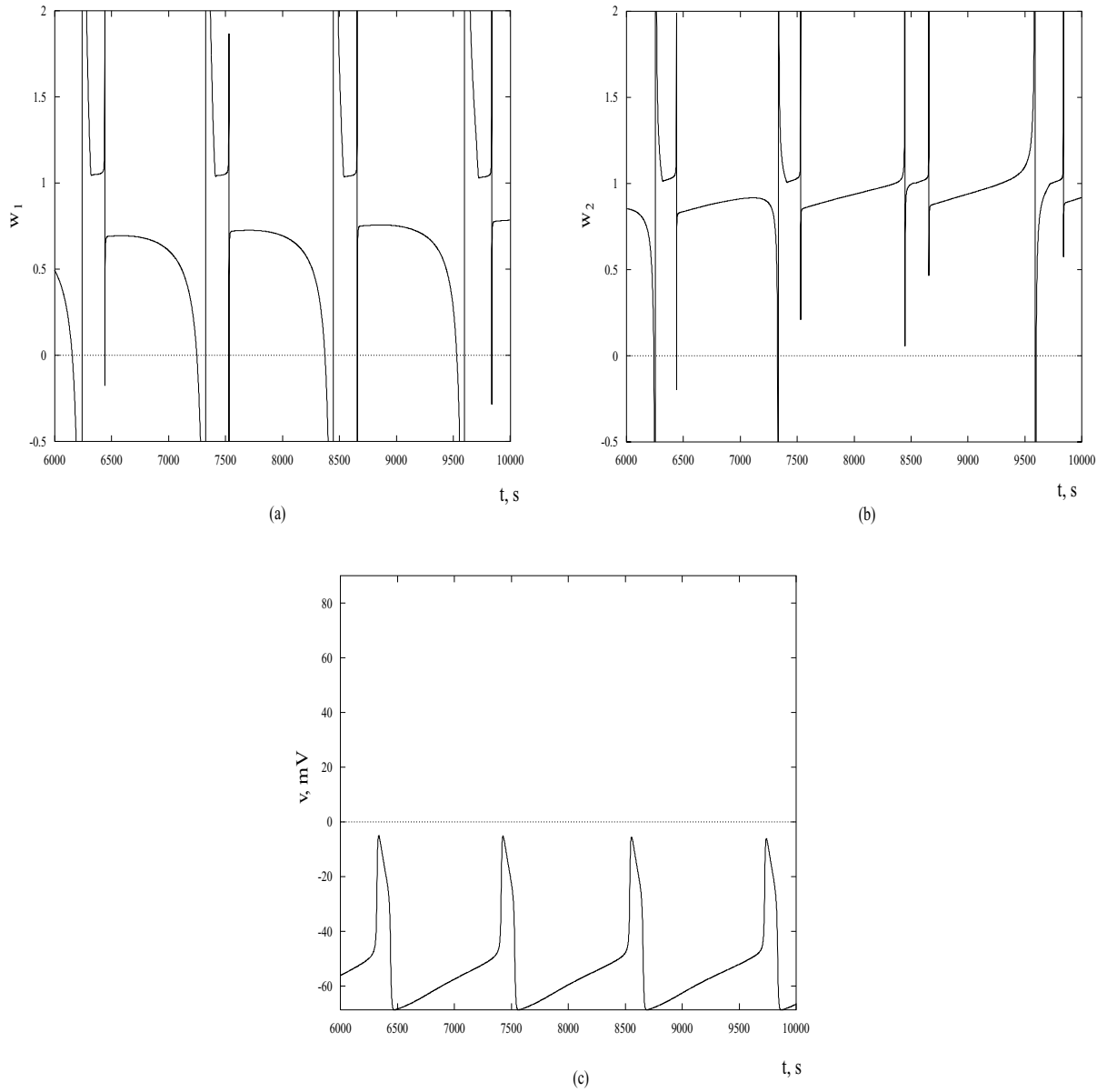


Figure 4. Plots (a) and (b) present the time series for the ratios of $\chi_i = \frac{G(v_i) - \gamma u_i}{G(v_{i+1}) - \gamma u_{i+1}}$, $i = 1, 2$, for the first two compartments of a five-compartment model. They are close to 1 for the most part of slow motion. Exceptions are the moments of time when the denominators become 0. (c) For reference, $v_1(t)$ is plotted for the same time interval.

the phase points move along the outer branches of the S-shaped nullclines (Fig. 5a) and “jump” to the opposite branches upon reaching the points of extrema (jump points). This description is completely analogous to the phase plane analysis for a single relaxation oscillator. For a more complete and rigorous discussion of the phase plane analysis for a closely related problem, we refer to the paper of Medvedev and Kopell (2001).

From Fig. 5a it is easy to see that the trajectories in the $v_1 - u_1$ and $v_1 - u_2$ phase planes converge to the limit cycles. Therefore, the voltage and calcium dynamics in the somatic and dendritic compartments are oscillatory. The shapes of the nullclines yield the waveforms and the amplitudes of oscillations. A simple inspection of (3.19), (3.21), and (3.22) implies that the ratio of amplitudes of calcium oscillations in the two compartments

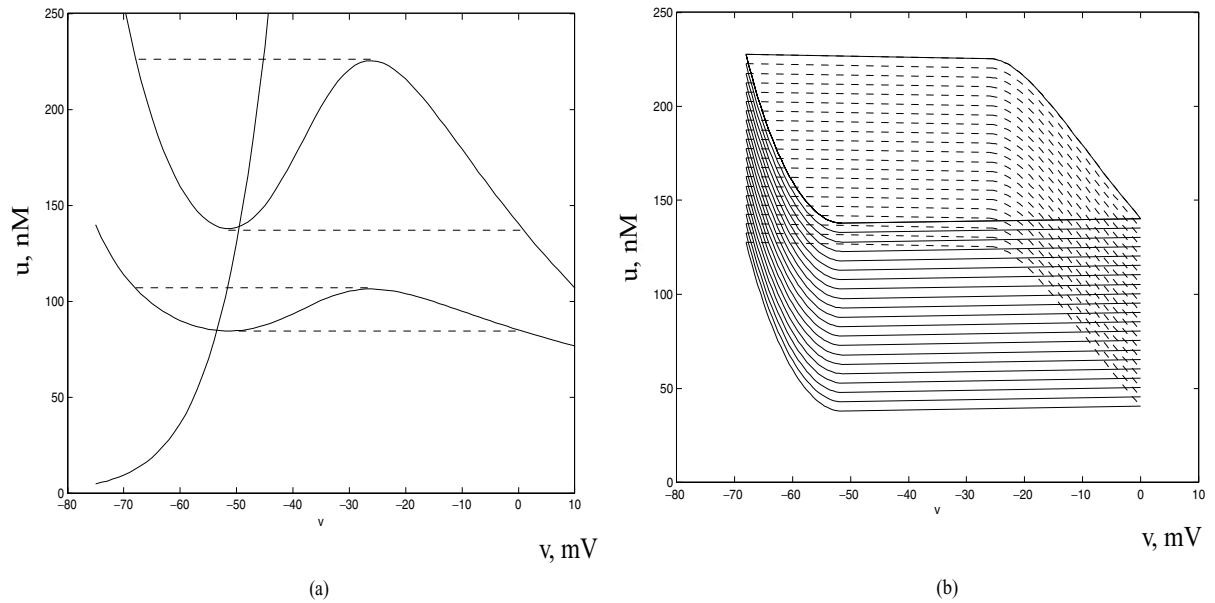


Figure 5. (a) The nullclines for voltage and calcium dynamics in the somatic and dendritic compartments are plotted in this figure. The forms of these nullclines are given by Eqs. (3.21) and (3.22) for fixed K . (b) A one-parameter family of periodic orbits forming a cylinder in the phase space.

is proportional to the ratio of their natural frequencies, i.e. $\omega_1 : \omega_2$. Thus, the dendritic compartment with smaller cross-sectional diameter and higher natural frequency has bigger amplitudes of calcium oscillations.

Above, we have assumed that the value of K is fixed in (3.21) and (3.22). The initial value of K is determined from the initial conditions. For finite intervals of time (and sufficiently large g), K can be considered as an ‘adiabatic invariant’ [3]. For longer times, the value of K must be adjusted for Eqs. (3.21) and (3.22) to remain a good approximation of the slow manifold. These adjustments result in a slow drift of the mean values of calcium oscillations. This creates slow transients in calcium dynamics, which are clearly seen numerically (Fig. 3b) and are also observed in the experimental data. Postponing the details of the transient dynamics until the next section, we present the geometric interpretation of the results of the present section: A union of the periodic orbits over all real K constitutes a one-parameter family (see Fig. 5b). Geometrically, this is a cylinder in a four-dimensional phase-space (the dimension of the phase space can be reduced to 3 if v_1 and v_2 are identified). This cylinder is important for describing solutions to (3.2)–(3.5): except possibly for some initial period of time the system dynamics is confined to the surface of this cylinder. Such surfaces, or mani-

folds (in higher dimensional spaces) are called *inertial manifolds*. In the next section, we study the system dynamics on the inertial manifold.

4. Transient Dynamics

In the present section, we develop techniques for tracking the system dynamics on the cylinder foliated by the periodic orbits (Fig. 5b). We will show that trajectories converge onto the limit cycle of the coupled system. It turns out that the rate of convergence and, therefore, the duration of transients depend on the interplay between two parameters: the strength of coupling, g , and the rate constant of calcium extrusion, γ . In the regime considered in this paper, we will show that it is the latter that determines the duration of transients.

We introduce a function:

$$L(u_1, u_2) = \frac{1}{2} \left(\frac{u_2}{\omega_2} - \frac{u_1}{\omega_1} + A \right)^2, \quad (4.1)$$

where the constant A will be specified below. $L(u_1, u_2)$ has several properties that are useful for studying the dynamics of (2.1) and (2.4). Our first observation is that L can be considered as a function of K . To show this, we calculate the linear combination on the right

hand side of (4.1), using (3.21) and (3.22):

$$\begin{aligned} & \frac{u_2}{\omega_2} - \frac{u_1}{\omega_1} + A \\ &= \left[\frac{1}{\omega_2} - \frac{\xi l}{\omega_2} - \frac{1}{\omega_1} - \frac{\xi r}{\omega_1} \right] f(v) - \kappa_1 K + A, \\ \kappa_1 &= \frac{l\omega_1 + r\omega_2}{\omega_1\omega_2} = \frac{\pi}{4\beta Rh} (d_1^3 + d_2^3). \end{aligned} \quad (4.2)$$

The expression in the square brackets is zero, as is easily seen from the definition of ξ (3.19). Hence,

$$\frac{u_2}{\omega_2} - \frac{u_1}{\omega_1} + A = -\kappa_1 K + A. \quad (4.3)$$

Equations (4.1) and (4.3) imply that L is a function of K . Namely,

$$L(K) = \frac{1}{2}(\kappa_1 K - A)^2. \quad (4.4)$$

Next we show that as the trajectories of (2.1), (2.4) approach the steady state oscillations, the values of $L(u_1, u_2)$ averaged over one period of oscillations monotonically decrease to zero. The rate of decay of L yields the duration of the transients and reveals the physiological factors that influence the rate of transients. For this, we compute

$$\frac{dL}{dt} = \left(\frac{u_2}{\omega_2} - \frac{u_1}{\omega_1} + A \right) \left(\frac{\dot{u}_2}{\omega_2} - \frac{\dot{u}_1}{\omega_1} \right), \quad (4.5)$$

where \dot{u} stands for $\frac{du}{dt}$. The first term on the right hand side of (4.5) is given by (4.3), and it remains to evaluate the second term. Using (3.5) and (3.9), we have

$$\frac{\dot{u}_2}{\omega_2} - \frac{\dot{u}_1}{\omega_1} = G(v_2) - G(v_1) - \gamma(u_2 - u_1), \quad (4.6)$$

$$\begin{aligned} G(v_2) - G(v_1) &\approx G'(v_1)(v_2 - v_1) \\ &= \delta\alpha G'(v_1)(E_K - v_1)c(v_1) \end{aligned} \quad (4.7)$$

and from (3.11) and (3.12) we obtain

$$u_2 - u_1 = -(l+r)c(v_1). \quad (4.8)$$

The combination of (4.6)–(4.8) and (3.20) yield

$$\begin{aligned} \frac{\dot{u}_2}{\omega_2} - \frac{\dot{u}_1}{\omega_1} &= (\delta\alpha G'(v_1)(E_K - v_1) \\ &\quad + \gamma(l+r))c(v_1) \end{aligned}$$

$$\begin{aligned} &= (\delta\alpha G'(v_1)(E_K - v_1) \\ &\quad + \gamma(l+r))(\xi f(v_1) + K). \end{aligned} \quad (4.9)$$

Assuming that the period of oscillations of the coupled system, T , does not change to leading order, we integrate the last expression over one period of oscillations to obtain

$$\begin{aligned} \int_0^T \left(\frac{\dot{u}_2}{\omega_2} - \frac{\dot{u}_1}{\omega_1} \right) d\tau &= (\delta F_1 + \gamma F_2)K + (\delta J_1 + \gamma J_2) \\ &= (\delta F_1 + \gamma F_2)(K - \kappa_2), \end{aligned} \quad (4.10)$$

where

$$\kappa_2 = \frac{-(\delta J_1 + \gamma J_2)}{\delta F_1 + \gamma F_2}; \quad (4.11)$$

$$F_1 = \int_0^T \alpha G'(v_1)(E_K - v_1) d\tau, \quad (4.12)$$

$$F_2 = (l+r)T, \quad (4.13)$$

$$\begin{aligned} J_1 &= \int_0^T \alpha \xi G'(v_1)(E_K - v_1) f(v_1) d\tau \\ &= \int_0^T \xi G'(v_1) \tilde{F}(v_1) d\tau, \end{aligned} \quad (4.14)$$

$$J_2 = (l+r)\xi \int_0^T f(v_1) d\tau. \quad (4.15)$$

We are now ready to calculate the change of L after one period of oscillations of (2.1), (2.4). For this we integrate (4.5) over one cycle and use (4.3) and (4.10)

$$\begin{aligned} \Delta L &= \int_0^T \frac{dL}{dt} dt \\ &= -\kappa_1 (\delta F_1 + \gamma F_2) \left(K - \frac{A}{\kappa_1} \right) (K - \kappa_2). \end{aligned} \quad (4.16)$$

Finally, by setting $A = \kappa_1 \kappa_2$, from (4.16) and (4.4) we derive

$$\Delta L = \int_0^T \frac{dL}{dt} d\tau = -\kappa_1 (\delta F_1 + \gamma F_2) (K - \kappa_2)^2, \quad (4.17)$$

$$L(K) = \frac{\kappa_1^2}{2} (K - \kappa_2)^2. \quad (4.18)$$

By taking the limit as $\delta \rightarrow 0$ in (4.17) and (4.18) and using (4.11), we obtain

$$\begin{aligned} \frac{\Delta L}{T} &= \frac{-\kappa_1 \gamma F_2}{T} (K - \bar{\kappa}_2)^2 \\ &= -\frac{2(l+r)\gamma}{\kappa_1} L(K), \end{aligned} \quad (4.19)$$

where

$$\bar{\kappa}_2 = \frac{-J_2}{F_2} = \frac{-\xi}{T} \int_0^T f(v_1) dt. \quad (4.20)$$

Note that κ_2 differs from $\bar{\kappa}_2$ by $O(\delta)$. (4.19) implies that $L(t)$ decays to zero exponentially fast. This corresponds to the gradual approach of the solutions of (2.1) and (2.4) to a limit cycle of the coupled system. The latter is to leading order determined by (3.21) and (3.22) with $K = \bar{\kappa}_2$. The rate of approach is characterized by the exponent $\frac{-2(l+r)\gamma}{\kappa_1}$, i.e., is proportional to the rate of the calcium efflux γ . Equation (4.19) yields the rate of change of L for two coupled oscillators. Our conclusions about the relation between the rate of calcium efflux and the duration of transients are verified numerically. Figures 6(a) and (b) show that $L(t)$ decays to zero exponentially fast. Furthermore, the rate of decay is in a good agreement with our theoretical prediction: $\frac{-2(l+r)\gamma}{\kappa_1}$. Therefore, in our range of parameters the duration of transients is determined by γ , the rate of calcium extrusion. If δF_1 is much larger than γF_2 , then the transient time becomes dominated by the strength of the coupling rather than the rate of efflux of the calcium. Thus there are different regimes, and changes of parameters can affect what governs the length of the transients. In general, when the number of oscillators exceeds two (4.19) is not valid. In this case, it can be

shown that $L(t)$ is bounded from above and below by two exponential functions with exponents proportional to γ . This can be done by following the steps of the analogous derivation in (Medvedev and Kopell, 2001).

For the steady state oscillations, the slow equations take form:

$$u_1 = (1 + r\xi)f(v_1) + r\bar{\kappa}_2, \quad (4.21)$$

$$u_2 = (1 - l\xi)f(v_1) - l\bar{\kappa}_2. \quad (4.22)$$

By integrating (4.21), (4.22) over one period of oscillations and recalling the definition of $\bar{\kappa}_2$ (4.20), it is easy to see that the calcium concentrations averaged over one cycle are equal in two compartments:

$$\frac{1}{T} \int_0^T u_1 dt = \frac{1}{T} \int_0^T u_2 dt = \frac{1}{T} \int_0^T f(v(t)) dt. \quad (4.23)$$

Therefore, the steady state oscillations are characterized by equal average concentrations in two compartments (the same conclusion also holds when the number of compartments is greater than two). This explains the nature of the transient dynamics: the transients are driven by the difference in calcium concentrations in neighboring compartments. If the coupling is sufficiently large, the rate of the transients is set by the rate of the calcium efflux, as shown above. In the

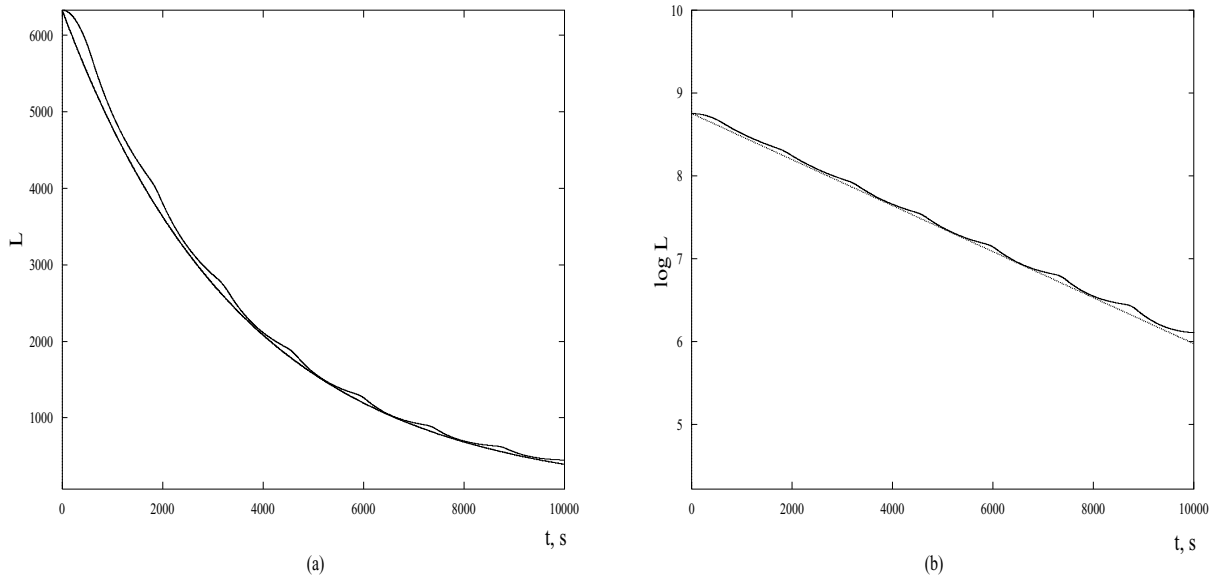


Figure 6. (a) L evaluated numerically along the trajectory of (2.1) and (2.4) and the analytical prediction for the exponential decay of $L(t)$ with exponent $\frac{-2(l+r)\gamma}{\kappa_1}$. (b) logarithm of the data in (a).

course of the transients the average calcium concentrations are equilibrated.

We can now justify the assumption (3.18), which was made earlier to simplify the analysis. Since the average calcium concentrations are equal in two compartments in the steady state, then close to the steady state u_1 and u_2 oscillate around a common mean value. When this mean value is high enough

$$\frac{G(v_1) - \gamma u_1}{G(v_1) - \gamma u_2} \approx 1,$$

despite the different amplitudes of oscillations of u_1 and u_2 . In this respect, our earlier assumption (3.18) combined with the later conclusions makes our analysis self-consistent.

5. Discussion

5.1. *Can the Dopaminergic Neuron be Treated as a Set of Discrete Oscillatory Compartments?*

Usually, compartmentalization of a dendritic neuron is a computational fiction, designed to escape the difficulty of solving a partial differential equation for the dendritic tree as a whole. In that case, it is important to keep the length of each compartment short and the change in diameter from compartment to compartment small, to approximate the limit for a continuously tapering dendrite. Because of the morphological features of the dopaminergic neuron and the properties of oscillatory dendrites, we have not taken that approach. The dendrites of the dopaminergic neuron change diameter mostly at branch points, and while they do taper between branches, these changes in diameter are small. In oscillatory dendrites, adjacent lengths of dendrite with the same diameter, and thus the same natural frequency, are strongly coupled and oscillate as a unit. Thus we suggest a view of the dopaminergic neuron as consisting of a relatively small number of discrete compartments, with discrete boundaries at dendritic branch points. Although the branch points themselves have not been considered in this paper, they are amenable to the approach we have taken. For branch points that give rise to approximately equal size daughter branches, coupling currents would be divided among the two daughter branches, but would be otherwise unchanged. This would double the effectiveness of the small diameter side of the junction among compartments. Small short side branches arising from large dendrites are also seen

on dopaminergic neurons. Because of the asymmetry of coupling currents, these will interact asymmetrically, with the larger dendrite dominating the activity of the smaller one. Both kinds of branching can be accommodated in the treatment here as an appropriate adjustment of the values for ρ_i .

5.2. *High Ca Concentrations in Dendrites may Contribute to Dendritic Release of Dopamine*

An important consequence of strong electrical coupling is the distortion of the calcium concentration time course, in which calcium concentrations in fine dendrites are driven to levels well in excess of those that would occur otherwise. This would not occur if dendrites were passive followers of the oscillation, or if they were free to oscillate at their own natural frequencies. The high calcium concentration observed in the dendrites during spontaneous membrane potential oscillations is the principal experimental evidence for the active participation of dendrites in the oscillatory mechanism. The large dendritic calcium transients may have physiological consequences. Dopamine release sites identified in electron microscopic studies have been principally in the finest dendritic branches (Wilson et al., 1977). Although a number of calcium-independent mechanisms for dopamine release in the substantia nigra have been proposed, most or all dopamine release observed experimentally is calcium-dependent, and occurs by vesicular exocytosis (Heeringa and Abercrombie, 1995; Rice et al., 1997). The high calcium concentration transients generated in small dendrites by the interaction of large and small diameter regions of the neuron may facilitate transmitter release in dendrites independently of action potential invasion into these fine branches of the dendritic tree. By acting on dopaminergic autoreceptors, dopamine released from the dendrites may contribute to generating the characteristic firing pattern of the dopamine neuron, and thus contribute to pattern of dopamine release at axon terminals in the same cells.

5.3. *Role of Backpropagating Action Potentials*

The calcium-based oscillations studied here are observed in dopaminergic neurons after blockade of action potential currents. In the absence of that blockade, single action potentials are generated on each cycle of the slow oscillation, and these have been reported to

propagate throughout at least the major branches of the dendritic tree (Hausser et al., 1995). The large currents associated with the action potential are certain to influence the coupling of compartments and may overwhelm the interactions studied here. In experimental studies, the presence of the backpropagating action potential had a relatively small effect on calcium concentration, or on the frequency of the membrane potential oscillation. The underlying membrane potential oscillation studied here neither depends upon the presence of the action potential, nor is it altered greatly in form or frequency when the action potential is present. It is possible that the action potential increases the effective electrical coupling among the various parts of the dopaminergic neuron's dendritic tree, synchronizing the cell for a brief period at the peak of each cycle. Under conditions of weaker electrical coupling than studied here this may be important to maintaining the coherence.

5.4. Propagation of Transients on the Dopaminergic Neuron

A perturbation of charge stored on the membrane localized to one part of the neuron (for example a synaptic potential) is usually thought to decay continuously with distance from the source due to redistribution of charge and loss through the membrane conductance. In the distributed oscillatory membrane of the dopaminergic neuron as envisioned here, such perturbations are best represented as a transient distortion of the voltage nullcline of the perturbed compartment. The propagation of the transient from one compartment to the next will not follow the rules of linear cable theory, and intuition based on familiarity with those rules will not be reliable. Perturbations propagate from one compartment to the next, but by way of coupled distortions of the mechanism of the oscillation. The principles that govern the interactions among synaptic inputs occurring at various location on the dendrites have not yet been determined, but the results of this study indicate that transients long enough to cause a deviation of calcium concentration from steady state values may take a long time to decay, with changes in voltage and calcium recovering at the time course of calcium concentration equilibration. Thus changes in firing of dopaminergic neurons, such as the response seen in the course of operant learning (Waelti et al., 2001) may be largely shaped by intrinsic mechanisms.

5.5. Adaptation of Oscillation Frequency and its Mechanism

The analysis presented here attempts only to explain the transient during establishment of oscillations with initial conditions far from the limit cycle. The voltage and calcium concentration changes for this kind of transient were collected by Wilson and Callaway (2000) and were available for comparison with the theoretical results. In the experiment, cells were hyperpolarized for several seconds to allow calcium concentration in the cell to fall well below steady state values. The hyperpolarizing current was removed and the cell allowed to evolve back to its steady state oscillation. The resulting transient was characterized by an initial higher than normal oscillation frequency which gradually slowed to the steady state value. During the approach to steady state, the somatic calcium concentration gradually approached its steady state cycle from below, while more distal dendrites had an initially high calcium concentration which gradually decreased, approaching the steady state from above. Throughout the transient, the amplitude of calcium oscillations were larger in the dendrites than in the soma. After achieving steady state, the calcium oscillations in the dendrites continued to be larger than the soma, but the calcium concentration averaged over a cycle was approximately the same in all measured parts of the cell. These results were duplicated in the model consisting of a chain of compartments with gradually increasing natural frequencies but synchronized by strong voltage coupling (Fig. 3). Examination of the phase trajectories in each compartment suggested that the trajectories were expanded (for the small compartments) or compressed (for the larger ones) along the [Ca] axis, and subject to a gradual drift (upward for the large compartments and down for the small ones) along the same axis. We show that the multi-dimensional system consisting of many compartments can be approximated as a set of uncoupled oscillators which have been subjected to an appropriate scaling on the [Ca] axis. The amplitude of scaling depends primarily upon the geometry of the neuron (the diameters of adjacent compartments). This distortion is due to the influence of coupling currents which must be added to the current balance equation of each compartment. The drift of trajectories over several cycles during the approach to steady state reflects the difference between average calcium concentration (averaged over a cycle of oscillation) and the steady state average. Because the coupled system oscillates faster than the natural

frequency of the soma, calcium concentration cannot achieve its steady state peak value on the first few cycles of the transient. Because the coupled system oscillates slower than the natural frequency of the distal dendrites, calcium concentration there overshoots on average. The small contribution of the large compartments' calcium-dependent potassium current (caused by the low calcium concentration) causes the smaller dendritic oscillations to dominate, and the oscillation frequency begins faster than steady state value. Somatic calcium concentration also does not have enough time to be pumped out between cycles, so it accumulates. Likewise, dendritic peak calcium concentrations have more than sufficient time to clear, and tend down. These average trends are reected in the translation of the voltage nullcline up the calcium axis for the large dendrites, and down for the small ones. The time required for this transient to decay is determined by the calcium clearance rate ($\beta\gamma$) and the difference in natural frequencies of the compartments (reflected in κ).

5.6. Related Mathematical Work

There is a very large literature related to the mathematical work in this paper. For example, chains of relaxation oscillators have been studied by Afraimovich and Chow (1997), Afraimovich et al. (1986), Belair and Holmes (1984), Hale (1997), Grasman (1984, 1987), Izhikevitch (2000), Kopell and Ermentrout (1986), Rand and Holmes (1980), Rubin and Terman (2000), Skinner et al. (1997), Somers and Kopell (1993, 1995), Storti and Rand (1986), Wang (1995), Wang and Rinzel (1995), and Wang and Terman (1995). Electrical coupling was studied in pairs or chains of oscillators in, e.g., (Chow and Kopell, 2000; Kopell et al., 1998; Manor et al., 1997; Sherman and Rinzel, 1992; Smolen et al., 1993; de Vries et al., 1998). It is known that strong coupling can lead to almost synchronous values of the coupled variables, even if the two elements being coupled are quite different (e.g., Afraimovich et al., 1986; Afraimovich and Chow, 1997; Kopell et al., 1998; Manor et al., 1997). However, if the individual oscillators are different, synchronization does not always take place even when coupling is very strong (Afraimovich and Chow, 1997; Wilson and Callaway, 2000).

The analyses done in this paper and in that of Medvedev and Kopell (2001) focus on the long transient dynamics and their origin in the large variation in natural frequency of the individual compartments.

Medvedev and Kopell showed that, for a chain of coupled FitzHugh-Nagumo, oscillators, in the limit of strong electrical coupling, the coupling currents go to a moderate size (not infinitesimal) voltage-dependent limit; this enabled them to reduce the analysis of the coupled system to that for a set of uncoupled compartments (Medvedev and Kopell, 2001). Other papers for which such reduction exists, for different mechanistic reasons include those of Somers and Kopell (1993) and Rotstein et al. (2003).

The analysis in the paper of Medvedev and Kopell (2001) revealed an unexpected structure in the limit of strong coupling: there is a family of periodic orbits whose union forms an invariant cylinder in the phase space, which is partitioned as the level sets of an integral. For coupling large but not infinite, this integral becomes a Lyapunov function, and there is motion on the invariant cylinder toward a unique limit cycle. In the current paper, we show that, with some approximations, the same structure exists in the Wilson-Callaway model. The analysis of this paper can be expanded to chains of $N > 2$ oscillators; see (Medvedev and Kopell, 2001) for the techniques. As shown in (Medvedev, 2002), for a variation in the equation for the slow variable, one can get the integral even when the coupling strength is finite; this creates a "continuous attractor" of periodic orbits, with memory of initial conditions encoded in the periodic orbit chosen.

Appendix A

In this appendix we provide more details on the asymptotic analysis of Section 3. Below we present asymptotic expansions of the solutions with respect to a small parameter δ and show that the results of Section 3 follow from retaining the leading order terms in these expansions.

The ansatz (3.8) implies that

$$\frac{g(v_2 - v_1)}{\alpha(E_K - v_1)} = O(1). \quad (\text{A.1})$$

On the slow manifold we define a function $c(v_1)$ along the phase trajectory $(v_1(t), u_1(t), v_2(t), u_2(t))$, $t \in \mathbb{R}^+$:

$$c(v_1) = \frac{g(v_2 - v_1)}{\alpha(E_K - v_1)}. \quad (\text{A.2})$$

From (A.2) we have

$$v_2 = v_1 + \delta \alpha c(v_1)(E_K - v_1). \quad (\text{A.3})$$

In addition, we assume that on the slow manifolds $c(v_1)$ can be expanded into the series:

$$c(v_1) = \sum_{i=0}^{\infty} \delta^i c_i(v_1). \quad (\text{A.4})$$

The combination of (A.3) and (A.4) yields the asymptotic expansion for v_2 . We now proceed to determine the unknown coefficients in (A.4). We only need to find the lowest order term $c_0(v)$ in this expansion. For this, we plug (A.2)–(A.4) into the equations for the slow manifolds (3.6) and (3.7). By extracting leading order terms in the resultant equations (i.e., formally, by setting $\delta = 0$), we arrive at (3.11) and (3.12). Similarly, we plug (A.2)–(A.4) into the dynamical equations (3.5), extract the $O(1)$ terms, and use the resultant equations to derive (3.14) and (3.15). Therefore, the results of Section 3 should be viewed as a leading order asymptotic approximation of the slow system's dynamics.

Acknowledgments

The Work was partially supported by NSF VIGRE grant DMS-9810783 and NSF grant DMS-9729992; by NCRR, NIH grant G12-RR03034; NIH grant NS42276; NSF grants 9706694.

References

- Afraimovich VS, Verichev NN, Rabinovich MI (1986) Stochastic synchronization of oscillations in dissipative systems. *Sov. Radiophys.* 29: 795–800.
- Afraimovich VS, Chow S-N, Hale JK (1997) Synchronization in lattices of coupled oscillators. *Physica D* 103: 442–451.
- Arnold VI (1996) *Geometrical Methods in the Theory of Ordinary Differential Equations*. Springer-Verlag, New York.
- Belair J, Holmes PJ (1984) On linearly coupled relaxation oscillators. *Quarterly of Appl. Math.* 42: 193–219.
- Chow C, Kopell N (2000) Dynamics of spiking neurons with electrical coupling. *Neural Computation* 12: 1643–1678.
- deVries G, Zhu HR, Sherman A (1998) Diffusively coupled bursters: Effects of heterogeneity. *Bull. Math. Biol.* 60: 1167–1200.
- Grasman J (1984) The mathematical modeling of entrained biological oscillators. *Bull. of Math. Biol.* 46: 407–422.
- Grasman J (1987) *Asymptotic Methods for Relaxation Oscillations and Applications*. Springer-Verlag, NY.
- Hale JK (1997) Diffusive coupling, dissipation, and synchronization. *J. of Dynamics and Dif. Eqns* 9: 1–52.
- Hausser M, Stuart G, Racca C, Sakmann B (1995) Axonal initiation and active dendritic propagation of action potentials in substantia nigra neurons. *Neuron* 15: 637–647.
- Heeringa MJ, Abercrombie ED (1995) Biochemistry of somatodendritic dopamine release in substantia nigra: An in vivo comparison with striatal dopamine release. *J. Neurochem.* 65: 192–200.
- Izhikevich EM (2000) Phase equations for relaxation oscillations. *SIAM J. Appl. Math.* 60: 1789–1804.
- Kopell N, Abbott L, Soto-Trevino C (1998) On the behavior of a neural oscillator electrically coupled to a bistable element. *Physica D* 121: 367–395.
- Kopell N, Ermentrout GB (1986) Symmetry and phaselocking in chains of weakly coupled oscillators. *Comm. Pure Appl. Math.* 39: 623–660.
- Kopell N, Ermentrout GB (2002) Mechanisms of phase-locking and frequency control in pairs of coupled neural oscillators. In: B Fiedler, ed. *Handbook on Dynamical Systems*. Elsevier, Amsterdam, pp. 3–54.
- Manor Y, Rinzel J, Segev I, Yarom Y (1997) Low amplitude oscillations in the inferior olive: A model based on electrical coupling of neurons with heterogeneous channel densities. *J. Neurophysiol.* 77: 2736–2752.
- Medvedev GS (2002) A multidimensional continuous attractor in a chain of coupled oscillators. Submitted.
- Medvedev GS, Kopell N (2001) Synchronization and transient dynamics in the chains of electrically coupled FitzHugh-Nagumo oscillators. *SIAM J. of Appl. Math.* 61: 1762–1801.
- Mishchenko EF, Kolesov YuS, Kolesov AYU, Rozov NKH (1994) *Asymptotic Methods in Singularly Perturbed Systems*. Consultants Bureau, New York and London.
- Rand RH, Holmes PJ (1980) Bifurcations of periodic motions in two weakly coupled van der Pol oscillators. *Int. J. Nonlinear Mech.* 15: 387–399.
- Rice ME, Cragg SJ, Greenfield SA (1997) Characteristics of electrically evoked somatodendritic dopamine release in substantia nigra and ventral tegmental area in vitro. *J. Neurophysiology* 77: 853–862.
- Rotstein HG, Kopell N, Zhabotinsky AM, Epstein IR (2003) A canard mechanism in systems of globally coupled oscillators. To appear in *J. Appl. Math.*
- Rubin J, Terman D (2000) Geometric analysis of population rhythms in synaptically coupled neuronal networks. *Neural Comp.* 12: 597–645.
- Sherman A, Rinzel J (1992) Rhythmogenic effects of weak electrotonic coupling in neuronal models. *Proc. Nat. Acad. Sci. USA* 89: 2471–2474.
- Skinner FK, Kopell N, Mulloney B (1997) How does the crayfish swimmeret system work? Insights from nearest-neighbor coupled oscillator models. *J. Comput. Neurosci.* 4: 151–160.
- Smolen P, Rinzel J, Sherman A (1993) Why pancreatic islets bursts but single β -cells do not. The heterogeneity hypothesis. *Biophysics J.* 64: 1668–1680.
- Somers D, Kopell N (1993) Rapid synchronization through fast threshold modulation. *Biol. Cybern.* 68: 393–407.
- Somers D, Kopell N (1995) Waves and synchrony in arrays of oscillators of relaxation and non-relaxation type. *Physica D* 89: 169–183.

- Storti SW, Rand RH (1986) The dynamics of two strongly coupled relaxation oscillators. *SIAM J. Appl. Math.* 46: 56–67.
- Waelti P, Dickinson A, Schultz W (2001) Dopamine responses comply with basic assumptions of formal learning theory. *Nature* 412: 43–48.
- Wang DL (1995) Emergent synchrony in locally coupled neural oscillators. *IEEE Trans. on Neural Networks* 6: 941–948.
- Wang XJ, Rinzel J (1995) Oscillatory and bursting properties of neurons. In: MA Arbib, ed. *Handbook of Brain Theory and Neural Networks*. MIT Press, Cambridge, MA. pp. 686–691.
- Wang DL, Terman D (1995) Global competition and local cooperation in a network of neural oscillators. *Physica D* 81: 148–176.
- Wilson CJ, Callaway JC (2000) A coupled oscillator model of the dopaminergic neuron of the substantia nigra. *J. Neurophysiol.* 83: 3084–3100.
- Wilson CJ, Groves PM, Fifkova E (1997) Monoaminergic synapses including dendro-dendritic synapses in the rat substantia nigra. *Exp. Brain Res.* 30: 161–174.